Journal of Molecular Structure 1226 (2021) 129350

Contents lists available at ScienceDirect

Journal of Molecular Structure

journal homepage: www.elsevier.com/locate/molstr

Synthesis, characterization, crystal structure, Hirshfeld surface analysis, antioxidant properties and DFT calculations of a novel pyrazole derivative: Ethyl 1-(2,4-dimethylphenyl)-3-methyl-5-phenyl-1*H*-pyrazole-4-carboxylate

S. Naveen [a], Karthik Kumara [b,f], A. Dileep Kumar [c], K. Ajay Kumar [c], Abdelkader Zarrouk [d], Ismail Warad [e], N.K. Lokanath [b,*]

[a] Department of Physics, Faculty of Engineering and Technology, Jain (Deemed-to-be University), Jain Global Campus, Bangalore 562 112, India
[b] Department of Studies in Physics, Manasagangotri, University of Mysore, Mysuru 570 006, India.
[c] Department of Chemistry, Yuvaraja's College, University of Mysore, Mysuru 570 005, India
[d] Laboratory of Materials, Nanotechnology and Environment, Mohammed V University, Faculty of Sciences,4Av. Ibn Battuta, PO B.P. 1014 Rabat, Morocco
[e] Department of Chemistry and Earth Sciences, PO Box 2713, Qatar University, Doha, Qatar.
[f] Department of Physics, School of Sciences, Jain (Deemed-to-be University), Bangalore 560 011, India

ARTICLE INFO

Article history:
Received 24 July 2020
Revised 25 September 2020
Accepted 26 September 2020
Available online 28 September 2020

Keywords:
Pyrazole
Cyclocondensation
Antioxidant
X-ray diffraction
Radical scavenging

ABSTRACT

An effective route for the direct synthesis of substituted pyrazole through 3+2 annulation method was described. (*E*)-ethyl 2-benzylidene-3-oxobutanoate was prepared from ethyl acetoacetate and benzaldehyde *via* Knoevenagel approach. The cyclocondensation reaction of (*E*)-ethyl 2-benzylidene-3-oxobutanoate with phenylhydrazine hydrochloride in acetic acid (30%) medium under reflux conditions produced directly ethyl 1-(2,4-dimethylphenyl)-3-methyl-5-phenyl-1*H*-pyrazole-4-carboxylate and was characterized using spectroscopic methods *viz* NMR, mass, UV-Vis, and CHN analysis. The compound obtained was crystallized using methyl alcohol solvent by slow evaporation method and the 3D molecular structure was confirmed using single crystal X-ray diffraction studies. The crystal structure is stabilized by intermolecular hydrogen bond of the type C-H•••O and π•••π stacking interactions. Further, the calculated ^{1}H-NMR, TD-SCF, HOMO/LUMO, MEP, Hirshfeld surface and Mulliken population analysis were compared with the experimentally analyzed data. The optimized theoretical structure parameters are in good agreement with the experimental X-ray structures. The compound was evaluated *in vitro* for its antioxidant susceptibilities through DPPH and hydroxyl radical scavenging methods.

1. Introduction

An interest in antioxidant activity of small molecules, to prevent the deleterious effects caused by free radicals in the human body, has gained the attention of the wider research community. Free radicals are believed to be associated with multiple disease conditions such as carcinogenesis, inflammation, mutagenesis, arthritis and cancer [1]. These conditions arise due to the oxidative stress resulting from an imbalance between free radical generation and their quenching [2]. The elimination of free radicals and related species helps to eradicate the oxidative stress thereby associated diseases [3]. Despite numerous attempts to search for more effective antioxidant agents, pyrazoles still remain as the scaffold of choice, because these class of compounds demonstrated utility in quenching of free radicals and hence, has tremendous potential for exploration as lead candidates for drug discovery against oxidative damage [4]. Literature reveals that, the synthesized series of 3,4-diaryl-4,5-dihydro-1*H*-pyrazoles [5], 3,5-bis(substituted) pyrazoles [6], phenyl dendritic-like oxidants with pyrazolines/pyrazoles [7], pyrazole linked isoxazoles/thiazoles [8], 3,5-diamino-4-(1,2-diarylsulfonylethyl)-4*H*-yrazoles [9], possess remarkable antioxidant properties. The synthetic 1*H*-indol-2-yl (3,5-substituted diphenylyrazol-1-yl)methanone analogues are reported to act as promising antioxidant molecules, as these scavenges 2,2-diphenyl-1-picrylhydrazyl (DPPH), 2,2-azino bis(3-ethylbenzothiazoline-6-sulfonic acid) (ABTS) radicals [10] and the insertion of pyrazole core to 2-(3-(4-hydroxy-3-methoxyphenyl)acryloyl)quinoxaline 1,4-dioxide enhanced the radical scavenging abilities [11].

* Corresponding author.
E-mail address: lokanath@physics.uni-mysore.ac.in (N.K. Lokanath).

https://doi.org/10.1016/j.molstruc.2020.129350
0022-2860/

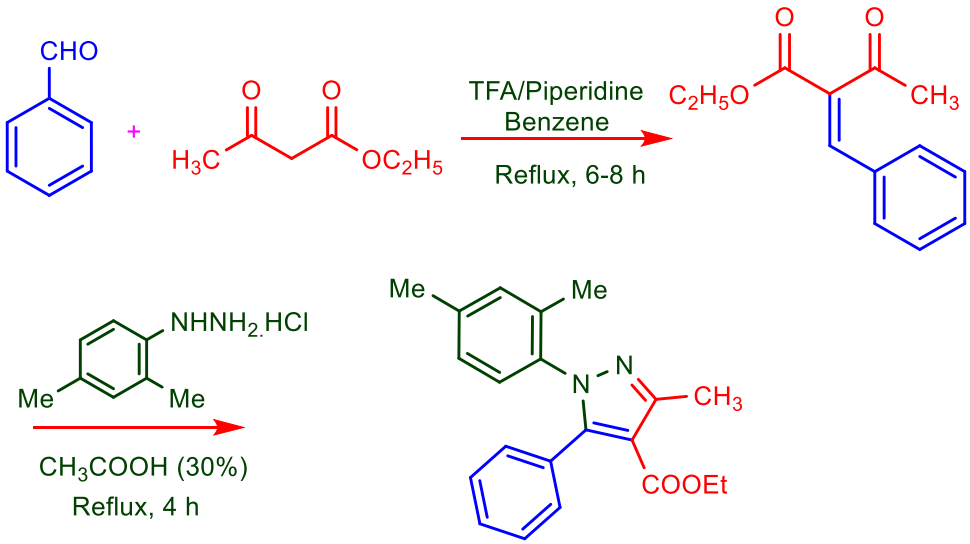

Fig. 1. Synthesis of ethyl 1-(2,4-dimethylphenyl)-3-methyl-5-phenyl-1*H*-pyrazole-4-carboxylate

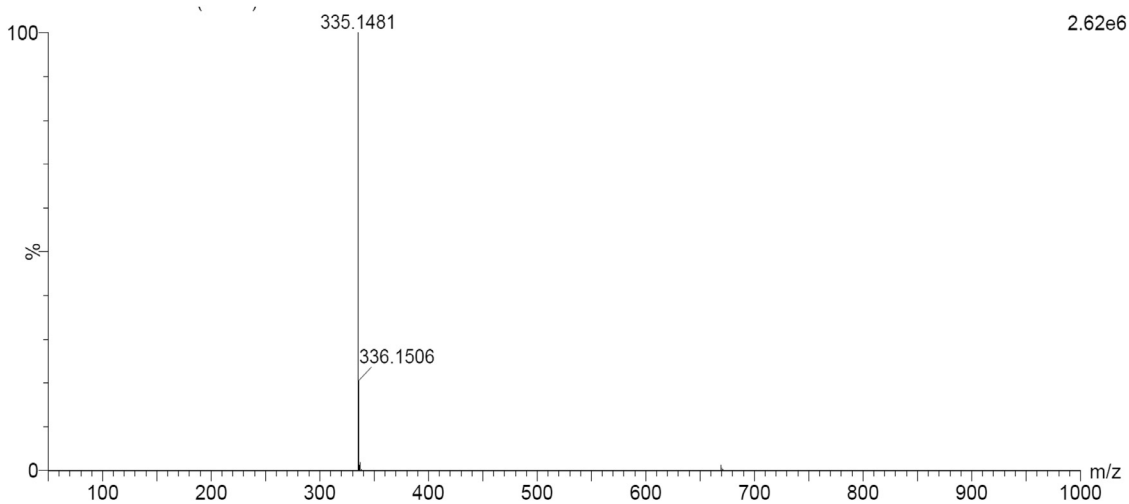

Fig. 2. TOF-MS spectrum of ethyl 1-(2,4-dimethylphenyl)-3-methyl-5-phenyl-1*H*-pyrazole-4-carboxylate

Development of novel and accessible procedure for the transformation of a simple molecule in to heterocycles is a worthwhile contribution in organic synthesis. Amongst the heterocycles, the compounds with pyrazole skeleton are the prominent class in active pharmaceutical drugs [12]. The reaction of substituted hydrazines with 1,3-dicarbonyl compounds in the presence of base, to produce pyrazoles through an intermediate *N*-alkyl/phenyl/acetyl hydrazino derivative was first reported [13]. The hydrazones prepared by the reaction of benzoyl-1-phenylhydrazine and active methylene compounds catalyzed by P_2O_5, followed by cyclisation in the base medium offered tetrasubstituted pyrazoles [14]. Highly regioselective synthesis of phosphonylpyrazoles, sulphonyl pyrazoles and carbonylated pyrazoles was achieved by the reaction of chalcones with α-diazo-β-ketophosphonate (Bestmanne Ohira Reagent, BOR) [15].

The drugs containing pyrazole nucleus demonstrated wide range of biological activities, such as antibacterial, anti-inflammatory, anticancer, anesthetic, analgesic, anti-convulsant [16-20] etc. They are also used in pharmaceutical drugs and agrochemicals in controlling infections, diseases and pests [21,22]. In view of the broad spectrum of synthetic and biological applications of pyrazoles and in search of new antioxidants, we herein report for the first time, the direct synthesis of a highly substituted pyrazole derivative, its spectral and crystallographic characterization, and the results of radical scavenging activities.

To the best of our knowledge, neither preparation nor computation studies on ethyl 1-(2,4-dimethylphenyl)-3-methyl-5-phenyl-1*H*-pyrazole-4-carboxylate have been carried out until now. The main aim of this study is to consolidate the X-ray structural and spectral properties of the title compound together with the computational analysis. In this study, XRD and optimized structure, vibrational spectra, electron transfer, TD-SCF, TOF-MS, ^{1}H, ^{13}C NMR, MEP, HOMO/LUMO, Hirshfeld surface and Mullikan population analysis were performed. Additionally, the antioxidant properties of the compound were evaluated by hydroxyl and DPPH methods. These computations and the experimental data of the molecule enrich prudence information upon pyrazole derivatives.

2. Experimental Section

2.1. Materials and Methods

Purity of the compound was checked on thin layer chromatography (TLC) plates pre-coated with silica gel using solvent system hexane**:** ethyl acetate (1:4). The spots were visualized under UV light. ^{1}H NMR (400 MHz) and ^{13}C NMR (100 MHz) spectra were

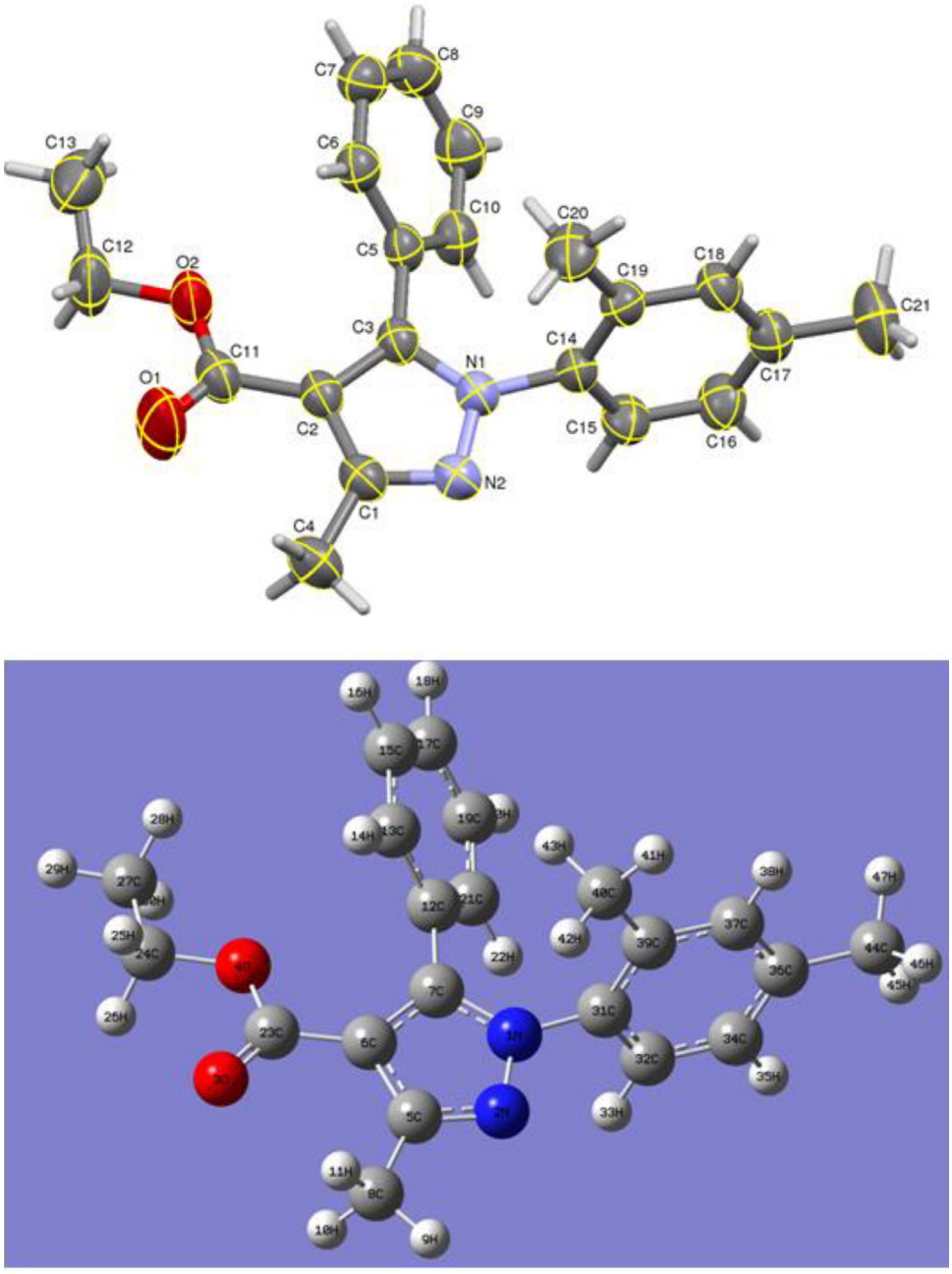

Fig. 3. (a) ORTEP with thermal ellipsoids drawn at 50% probability and (b) DFT- optimized mononuclear structure of the title compound.

recorded on Agilent-NMR spectrometer using solvent $CDCl_3$ and internal standard TMS. The chemical shifts are expressed in δ ppm. Mass spectrum was obtained on Mass Lynx SCN781 spectrometer TOF mode. Elemental analysis was obtained on a Thermo Finnigan Flash EA 1112 CHN analyzer.

*2.2. Synthesis of ethyl 1-(2,4-dimethylphenyl)-3-methyl-5-phenyl-1*H *pyrazole-4-carboxylate*

A solution mixture of (*E*)-ethyl 2-benzylidene-3-oxobutanoate (2.18 g, 10 mmol) and (2,4-dimethylphenyl)hydrazine hydrochloride (1.72 g, 10 mmol) in acetic acid (30%) was refluxed on a water bath for 4 h. The progress of the reaction was monitored by TLC. After the completion, the reaction mixture was cooled and poured into ice cold water. The solid separated was filtered, washed thoroughly with ice cold water. The crude solid was recrystallized from methyl alcohol to obtain target molecule in 90% yield; m.p., 108–109° C. MS (*m/z*): 335 (MH+, 100); Anal. Calcd. for $C_{21}H_{22}N_2O_2$ (%): C, 75.42; H, 6.63; N, 8.38; Found: C, 75.39; H, 6.59; N, 8.30. ^{1}H NMR ($CDCl_3$; δ ppm): 1.107-1.142 (t, 3H, CH_3), 1.934 (s, 3H, CH_3), 2.249 (s, 3H, CH_3), 2.565 (s, 3H, CH_3), 4.124-4.178 (q, 2H, CH_2), 6.906-7.248 (m, 8H, Ar-H); ^{13}C NMR ($CDCl_3$; δ ppm): 14.02 (1C, CH_3), 14.29 (2C, CH_3), 21.34 (1C, CH_3), 59.71 (1C, OCH_2), 111.81 (1C, C-4), 125.30 (2C), 126.76 (1C), 127.49 (1C), 128.57 (2C), 128.69 (2C), 130.26 (2C), 138.74 (1C), 139.30 (1C), 146.54 (1C, C-5), 151.63 (1C, C-3), 163.85 (1C, C=O).

2.3. Computational details

All calculations were made by Gaussian 09 software [23]. Gauss View 5 software was used to visualize the optimized structures [24]. X-ray structure coordinates were taken as starting point for

Table 1
Crystal data and structure refinement details.

Parameter	Value
CCDC number.	CCDC 2018644
Empirical formula	$C_{21}H_{22}N_2O2$
Formula weight	334.41
Temperature	293(2) K
Wavelength	1.54178 Å
Crystal system, space group	Monoclinic, $P2_1/c$
Unit cell dimensions	a = 12.8596(17) Å, b = 8.1101(11) Å c = 18.302(3) Å and β = 95.966(8)°
Volume	1898.4(5) Å^3
Z, Calculated density	4, 1.170 Mg/m^3
Absorption coefficient	0.602 mm^{-1}
$F_{(000)}$	712
Crystal size	0.24 × 0.21 × 0.20 mm
Theta range for data collection	4.86° to 64.55°
Limiting indices	-14≤ h ≤ 15, -9≤ k ≤9, -20≤ l ≤19
Reflections collected / unique	15373 / 3134[R(int) = 0.0688]
Refinement method	Full-matrix least-squares on F^2
Data / restraints / parameters	3134 / 0 / 230
Goodness-of-fit on F^2	1.055
Final R indices [$I>2\sigma(I)$]	$R1$ = 0.0740, $wR2$ = 0.2082
R indices (all data)	$R1$ = 0.0826, $wR2$ = 0.2214
Largest diff. peak and hole	0.316 and -0.332 e. Å^{-3}

theoretical calculations. Crystal Explorer 17.5 program was used to perform the Hirshfeld surfaces analysis [25].

2.4. X-ray diffraction studies

X-ray intensity data were collected at a temperature of 296 K on a Bruker Proteum2 CCD diffractometer equipped with an X-ray generator operating at 45 kV and 10 mA, using CuK_α radiation of wavelength 1.54178 Å. A complete data set was processed using *SAINT PLUS* [26]. The structure was solved by direct methods and refined by full-matrix least squares method on F^2 using *SHELXS* and *SHELXL* programs [27]. The geometrical calculations were performed using the program *PLATON* [28].

2.5. Antioxidant activities

2.5.1. DPPH radical scavenging activity

Antioxidants are characterized by their ability to scavenge the free radicals. Proton radical scavenging action is an important attribute of antioxidants, which is measured by DPPH scavenging assay [2]. 1 mL of DPPH solution (0.1mM in 95% methanol) was mixed with different aliquots of test samples (20, 40, 60, 80 and 100 μg/ml) in methanol. The mixture was shaking vigorously and allowed to stand for 20 min at room temperature. The absorbance was read against blank at 517 nm with ELICO SL 159 UV visible spectrophotometer. The free radical scavenging potential was calculated as a percentage (I %) of DPPH decolouration using the equation

I% of scavenging = $(A_0\text{-}A_1/A_0) \times 100$

Table 2
All the experimental XRD bond lengths (Å) and angles (°) with the DFT/B3LYP/6–311G(d) calculated values.

Bonds		Exp. XRD	B3LYP/6–311+ G(d,p)	Angles			Exp. XRD	B3LYP/6–311+ G(d,p)
N1	N2	1.364	1.3675	N2	N1	C3	113.1	112.73
N1	C3	1.354	1.3662	N2	N1	C14	117.9	118.05
N1	C14	1.436	1.4357	C3	N1	C14	128.9	129.19
N2	C1	1.317	1.3263	N1	N2	C1	105.1	105.52
O1	C11	1.198	1.2194	C11	O2	C12	117.7	115.8
O2	C12	1.443	1.4435	N2	C1	C2	111.2	110.94
C1	C2	1.409	1.4276	N2	C1	C4	119.5	120.14
C1	C4	1.501	1.4969	C2	C1	C4	129.2	128.92
C2	C3	1.399	1.4018	C1	C2	C3	105.7	105.37
C2	C11	1.465	1.4676	C1	C2	C11	123.9	123.73
C3	C5	1.476	1.4784	C3	C2	C11	130.4	130.78
C5	C6	1.387	1.4046	N1	C3	C2	104.9	105.44
C5	C10	1.387	1.4033	N1	C3	C5	121.9	122.45
C6	C7	1.379	1.3935	C2	C3	C5	133.2	132.1
C7	C8	1.372	1.397	C3	C5	C6	120.5	120.27
C8	C9	1.368	1.3953	C3	C5	C10	121.3	120.95
C9	C10	1.387	1.3948	C6	C5	C10	118.2	118.78
C14	C15	1.377	1.3938	C5	C6	C7	120.7	120.58
C14	C19	1.385	1.4052	C6	C7	C8	120.6	120.19
C15	C16	1.378	1.3932	C7	C8	C9	119.5	119.68
C16	C17	1.368	1.3987	C8	C9	C10	120.6	120.23
C17	C18	1.38	1.4008	C5	C10	C9	120.5	120.55
C17	C21	1.506	1.5112	O1	C11	O2	122.1	122.68
C18	C19	1.388	1.3984	O1	C11	C2	122.7	123.99
C19	C20	1.505	1.5088	O2	C11	C2	115.1	113.32
				O2	C12	C13	109	107.4
				N1	C14	C15	118.2	118.26
				N1	C14	C19	120.5	120.62
				C15	C14	C19	121.1	121.05
				C14	C15	C16	120	120.15
				C15	C16	C17	120.8	120.47
				C16	C17	C18	118.4	118.23
				C16	C17	C21	120.7	121.25
				C18	C17	C21	121	120.51
				C17	C18	C19	122.8	122.7
				C14	C19	C18	117	117.38
				C14	C19	C20	122	121.78
				C18	C19	C20	120.9	120.84

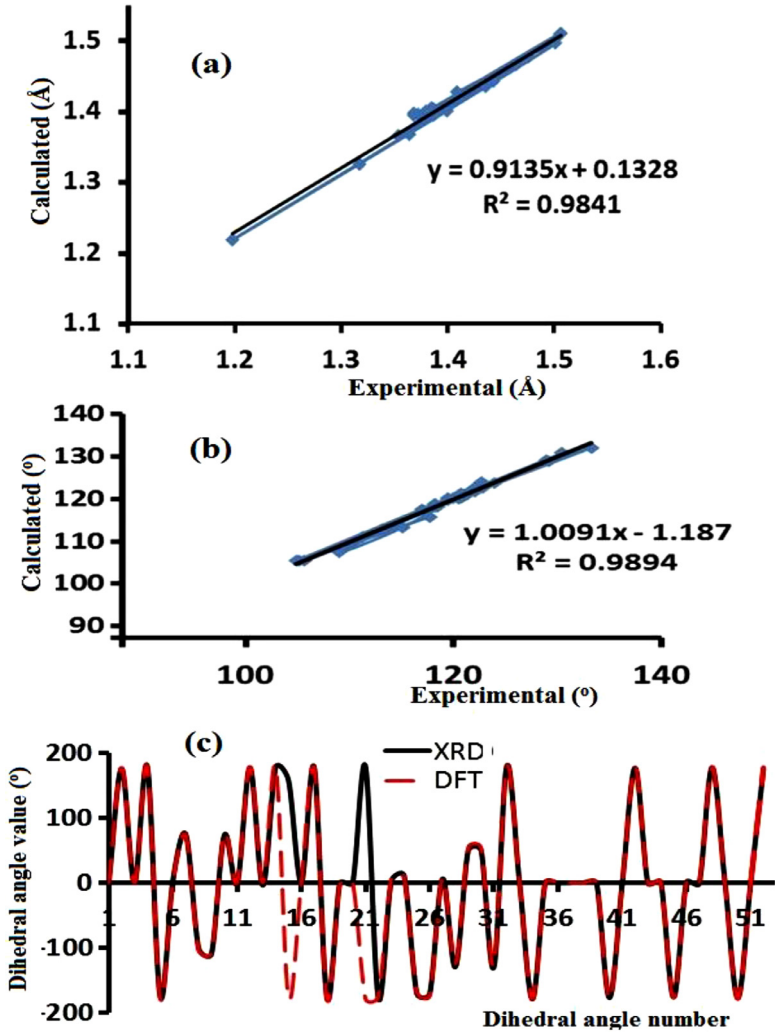

Fig. 4. XRD experimental structural parameters compared to DFT/B3LYP/6–31G(d) corresponding optimized data (a) bond lengths (b) bond angles and (c) torsion angles.

Where A_0 is the absorbance of the control reaction mixture excluding the test compounds and A_1 is the absorbance of the test compounds. Tests were carried out in triplicate and the results are expressed as I% ± standard deviations.

2.5.2. Hydroxyl radical scavenging activity

Hydroxyl radical scavenging assay was carried out according to the procedure reported earlier [29]. The product formed by degraded deoxyribose on heating with thiobarbituric acid (TBA) formed a pink colored chromogen confirming the formation of OH•. With the addition of test compound to the reaction mixture, they separate the hydroxy radicals from the deoxyribose and prevent their degradation. This experiment was performed by mixing 0.1 ml of phosphate buffer; 0.2 ml of 2-deoxyribose, test solution (20, 40, 60, 80 and 100 μg/ml) 0.1 ml of H_2O_2 (10 mM), 0.1 ml of ascorbic acid (1 mM), 0.1 ml of EDTA and 0.01 ml of $FeCl_3$ (100 mM) was incubated at 37°C for 60 min. Thereafter, the reaction was terminated by adding 1ml of cold 2.8% trichloroacetic acid and the reaction product was measured by adding 1 ml of 1% thiobarbituric acid (1 g in 100 ml of 0.05 N NaOH) in boiling water for 15 min. The absorbance was measured at 535 nm with BHA as a positive control. Decreased absorbance of the reaction mixture indicates increased hydroxyl radical scavenging activity.

3. Results and discussion

3.1. Chemistry

Initially, the intermediate (*E*)-ethyl 2-benzylidene-3-oxobutanoate, was synthesized by Knoevenagel reaction of ethyl acetoacetate with benzaldehyde in presence of catalytic amount of piperidine and trifluoroacetic acid. The cyclocondensation reaction of (*E*)-ethyl 2-benzylidene-3-oxobutanoate with (2,4-dimethylphenyl)hydrazine hydrochloride in acetic acid (30%) under reflux conditions produced ethyl 1-(2,4-dimethylphenyl)-3-methyl-5-phenyl-1*H*-pyrazole-4-carboxylate (Fig. 1).

Spectroscopic, MS and elemental analysis provided the structure proof of the ethyl 1-(2,4-dimethylphenyl)-3-methyl-5-phenyl-1*H*-pyrazole-4-carboxylate. Further, the single crystal X-ray diffraction study was also performed.

3.2. Mass and elemental analysis

The TOF-MS and elemental analysis of the title compound were consistent with the proposed molecular formula. Fig. 2 shows the molecular ion peak (MH+) as base peak at *m/z*: 335 correspond to its real molecular mass (calculated 334). The elemental analysis of $C_{21}H_{22}N_2O_2$ formula revealed Calcd: C, 75.42; H, 6.63; N, 8.38%, found. C, 75.39; H, 6.59; N, 8.30%. The MS and elemental analysis

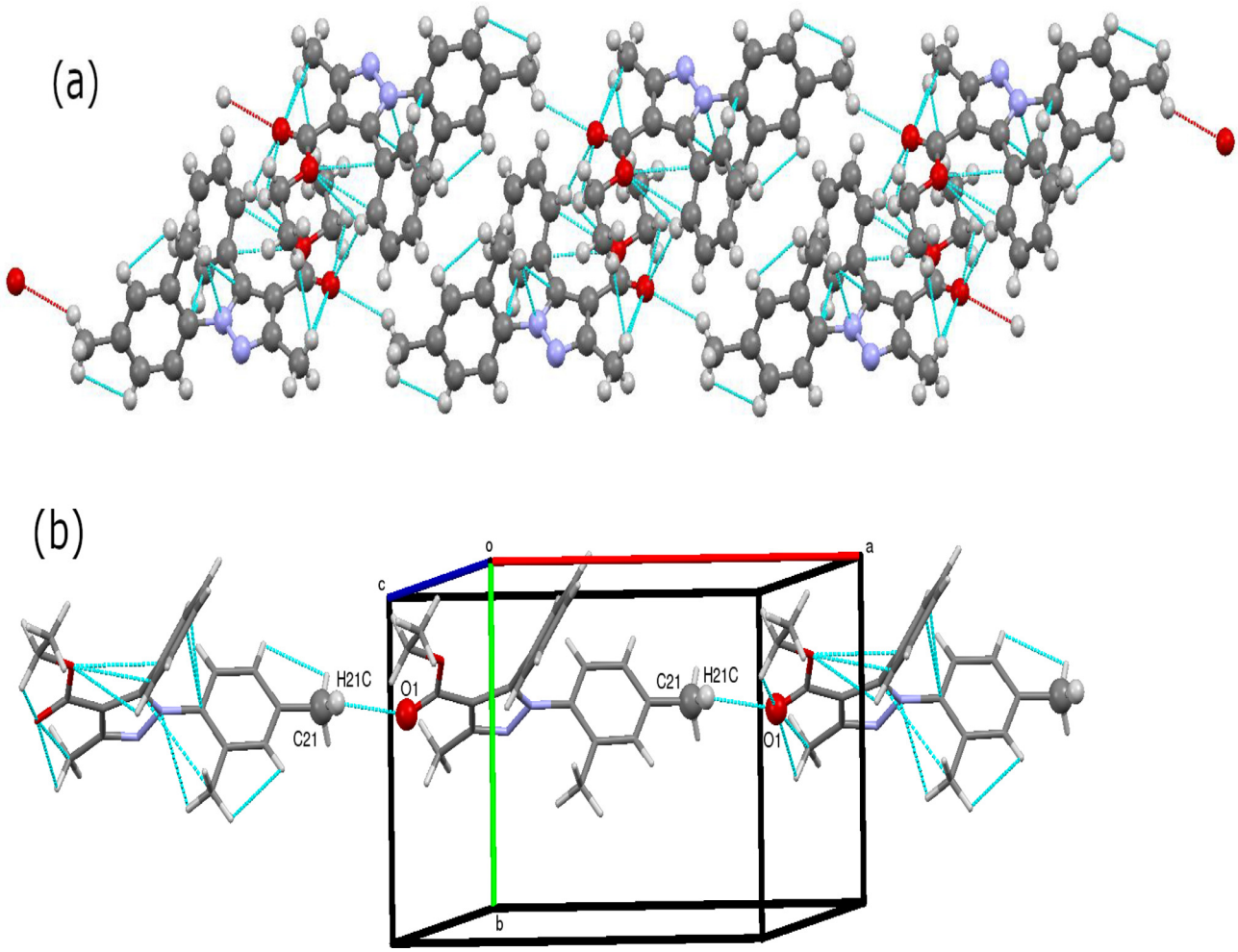

Fig. 5. (a) C—H…O hydrogen bonds connect the molecules forming 2D long chains (b) packing of molecules through C21-H21C-O1 intermolecular interactions.

showed satisfactory data consistent with the single crystal X-ray solved structure.

3.3. X-ray diffraction studies

The ethyl 1-(2,4-dimethylphenyl)-3-methyl-5-phenyl-1*H*-pyrazole-4-carboxylate compound (CCDC #: 2018644) was crystallized from methyl alcohol to give very light yellow crystals suitable for single crystal X-ray measurements. The details of the crystal structure and data refinement are given in Table 1. The ORTEP diagram of the molecule with thermal ellipsoids drawn at 50% probability is shown in Fig. 3**a.**

The title compound consists of three aromatic rings in which one is a five membered ring and two are six membered phenyl rings. The five membered pyrazole ring (N1/N2/C1/C2/C3) is the central core of the structure with dimethyl phenyl ring (C14/C15/C16/C17/C18/C19) at the N1 position and the plane phenyl ring (C5/C6/C7/C8/C9/C10) at the 5 position. Apart from these rings methyl group (C4-H_3) is substituted at the 3 position and the ethoxy carboxylate (C11=O1-O2-C12-(H_2)-C13-(H_3)) chain attached at the 4 position of the ring. Further, the planarity of the aromatic rings can be described based on the sigplan values [30] calculated for each ring using the below equation,

$$Sigplan = \sqrt{\sum_{j=1}^{n} d_j^2 / (N-3)}$$

Where, d_j is deviation of an atom j, the shortest distance from this atom to the plane of the ring for which the planarity to be defined and N is the maximum number of atoms present in the ring. All the aromatic rings are planar with the sigplan value of 0.004, 0.003 and 0.006 for pyrazole, phenyl and dimethyl phenyl rings respectively. The structural parameters are in good agreement with the similar structure reported earlier [31,32]. The molecular structure is non-planar which can be confirmed by analyzing the dihedral angles between the rings. The pyrazole ring makes dihedral angles of 49.97(13)º and 74.73(13)º with the phenyl and dimethyl phenyl rings, respectively. The dihedral angle between the phenyl and dimethyl phenyl rings is 68.25(11)º. These values confirm that the phenyl rings are out of plane with respect to the plane of the pyrazole ring. The methyl group is in the same plane of the ring as indicated by the torsion angle value of 178.2(2)° for N1-N2-C1-C4. The pendant ethoxy carboxylate chain is slightly out of plane with respect to the plane of the pyrazole ring as confirmed by the torsion angle values of 6.3(1)º and -170.9(2)° for C3-C2-C11-O2 and C1-C2-C11-O2 respectively.

The optimization of the structural coordinates of desired compound were performed using DFT method at B3LYP/6-311꞉G(d) level and the bond lengths and bond angles are compared with the experimental data as seen in Table 2 and Fig. 3b. Plotting of the X-ray experimental bond length (Fig. 4a) and bond angles (Fig. 4b) versus the corresponding theoretical data revealed an excellent matching with correlation coefficient R^2 = 0.9841 and 0.9894 respectively. The torsion angle values were also calculated at B3LYP/6-311꞉G(d)

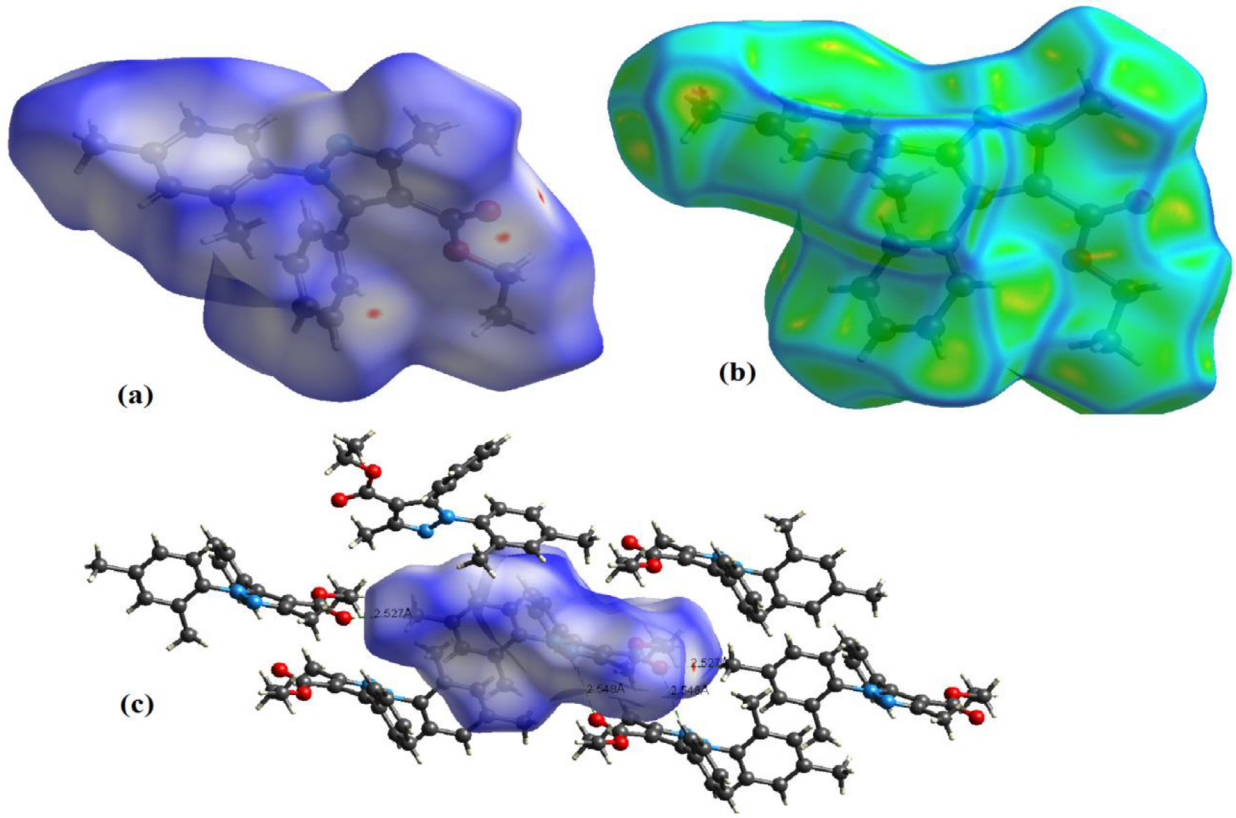

Fig. 6. (a) d_{norm}, (b) curvedness and (c) 3D H-Bonds network on Hirshfeld surface of compound.

as listed in Table 3. Most of the optimized torsion angles are very close in their values and orientations to the XRD experimental analysis except for angles C11-O2-C12-C13 and C1-C2-C3-C5 which have an opposite orientation (Fig. 4).

Four short polar contacts per molecule were detected, two C—H_{ph}...O=C and two C—H_{CH3}...O=C hydrogen bond links the molecules together. The molecules are packed in the crystal structure with two classical H-bonds types: C—H_{ph}...O=C (2.548 Å) and C—H_{CH3}...O=C (2.527 Å) as shortest and strongest H-bond Fig. 5(a). The crystal structure is stabilized by intermolecular hydrogen bond interactions of the type C-H...O; C(6)-H(6)...O(1) interaction with D...A distance of 3.434(4) Å, H...A distance of 2.55 Å, D-H...A angle of 159º with symmetry code *-x,1 -y, 1-z*. Similarly, C(21)-H(21C)…O(1) interaction with D...A distance of 3.285(4) Å, H...A distance of 2.53 Å, D-H...A angle of 136º with symmetry code *1+x, y, z* form 1D chain as shown in Fig. 5(b). Further, the crystal structure is also stabilized by π•••π interaction; Cg2•••Cg3 (Cg 2 is the centroid of the ring (C5/C6/C7/C8/C9/C10) and Cg3 is the centroid of the ring (C14/C15/C16/C17/C18/C19) with $\alpha = 68.25°$, $\beta = 50.1°$, $\gamma = 40.6°$, a perpendicular distance of Cg2 on ring Cg3 is 3.0197(9) Å and a Cg•••Cg distance of 4.0526(19) Å with symmetry code x, *y, z* [33,34].

3.4. Hirshfeld surfaces analysis (HSA)

The interaction between molecules in the crystal lattice of the desired compound was determined further more by HSA. Since the ethyl 1-(2,4-dimethylphenyl)-3-methyl-5-phenyl-1*H*-pyrazole-4-carboxylate compound contains oxygen and nitrogen atoms in its backbone which may act as H-bond acceptors, several H-bonds interactions were expected to be formed as red spots on the HSA surface of the molecule. On the HSA surface of the desired molecule, four remarkable interactions per molecule were detected as shown in the d_{norm} mapped Fig. 6a, two for C=O…..H_{CH3}, and two for C=O…..H_{ph}, N–H…N- interaction was detected in the desired molecular surface, see Fig. 6b. These 3D H-bonds network interaction played critical role in crystal stabilization [35-37]. The HSA interactions are consistent with the X-ray crystal packing data.

The finger-print plot (FP) highlights the most important intermolecular contacts. The FP analysis revealed the H/H intermolecular as largest contributor contacts with 81.1%. The 2D-FP plots over the Hirshfeld surfaces showed the presence of inter-contacts as the following order: H…H > H…C > H…O > H…N, as depicted in Fig. 7.

In experimental ^{1}H NMR spectra in $CDCl_3$ solvent, a triplet for three protons at δ 1.124 ppm due to CH_3 of ester protons, three singlets for the other CH_3 protons were signalled as singlet at δ 1.934, 2.249 and 2.565 ppm. A quartet for two protons OCH_2 was observed at δ 4.151 ppm. The protons of the benzene ring resonate as singlet, doublet and doublet of doublet at δ 6.906-7.248 ppm as seen in Fig. 8a. The ^{1}H NMR values of the compound were well within the spectral region of the reported structurally related compounds. For instance, ethyl 5-benzoxyl-4-*p*-tolyl-4*H*-pyrazole-3-carboxylate reported by D. Nair *et al* [38], showed the signals as triplet at δ 1.24 ppm for ester CH_3, and singlet at δ 2.31 ppm for Ar-CH_3, quartet at δ 4.30 ppm, array of singlet, doublet and multiplet at δ 7.08-7.86 ppm for aromatic protons. The reported compound ethyl 1-(2,4-dimethylphenyl)-5-(4-fluorophenyl)-3-methyl-1*H*-pyrazole-4-carboxylate showed the signals as triplet at δ 1.21 ppm for ester CH_3, three singlets at δ 1.95, 2.31, and 2.54 ppm for Ar-CH_3, and pyrazole-CH_3 protons, also a quartet at δ 4.21 ppm, and an array of signals at δ 7.29-7.60 ppm for aromatic protons [39]. Theoretical ^{1}H NMR in gaseous state using NMR-DB and ACD-LAB were compared with the experimental ^{1}H NMR as seen in Fig. 8b and Fig. 8. The theoretical ^{1}H NMR (chemical shifts and splitting) showed a very good matching with the experimental re-

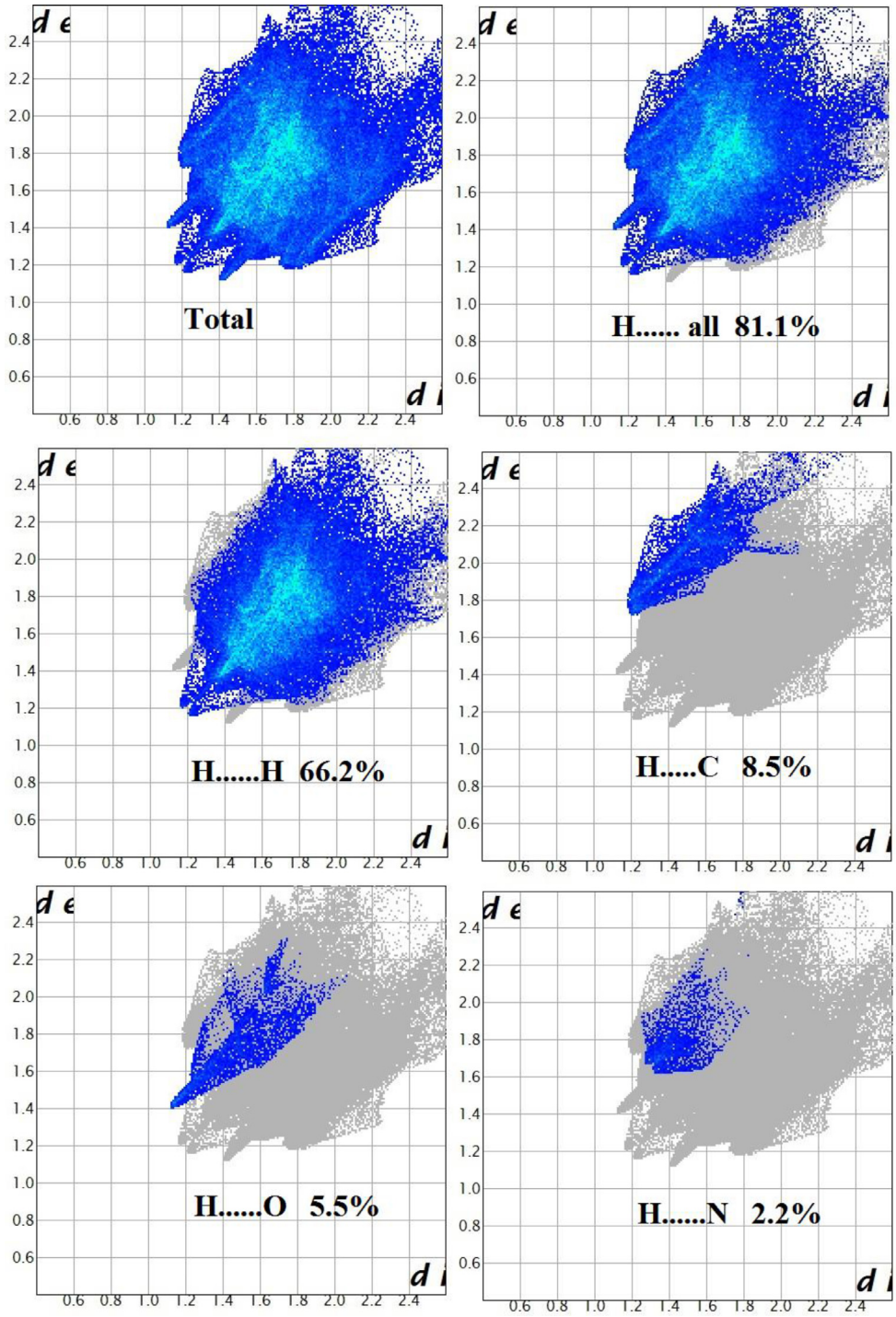

Fig. 7. Atom $_{inside}$…Atom $_{outside}$ FP plots of the compound.

sults as seen in Fig. 9. Better resolution was collected by ACD-LAB, plotting the ^{1}H NMR calculated chemical shifts collected by ACD-LAB versus the experimental gave significant $R^2 = 0.9266$ (Fig. 9a), while NMR-DB revealed the correlation coefficient of $R^2 = 0.9139$ (Fig. 9b).

In the ^{13}C NMR spectrum, the designed compound showed the resonance signals at δ 14.02, 14.29 (2C), and 21.34 ppm for four CH_3, at δ 59.71 ppm for OCH_2 and at δ 163.85 ppm for ester C=O carbons. The carbons of newly formed pyrazole ring C-4, C-5 and C-3 absorbed correspondingly at δ 111.81, 146.54 and 151.63 ppm. A spectrum of signals absorbed for two carbons each at δ 125.30, 128.57, 128.69, 130.26 ppm and for one carbon each at δ 126.76, 127.49, 138.74 and 139.30 ppm were unambiguously assigned to aromatic carbons. The ^{13}C NMR values of the compound were in good agreement with the structurally related molecule ethyl 1-(2,4-dimethylphenyl)-5-(4-fluorophenyl)-3-methyl-1*H*-pyrazole-4-carboxylate [39], which showed the resonance signals at δ 14.2, 14.3, 15.7, and 20.9 ppm for four CH_3, at δ 60.3 ppm for OCH_2 and at δ 163.2 ppm for ester carbonyl carbons. The C-4, C-5, and C-3 carbons of pyrazole ring showed signals at δ 112.4, 141.6 and 151.3 ppm, and an array of signals in the region of δ 117.8-159.4 ppm for aromatic carbons.

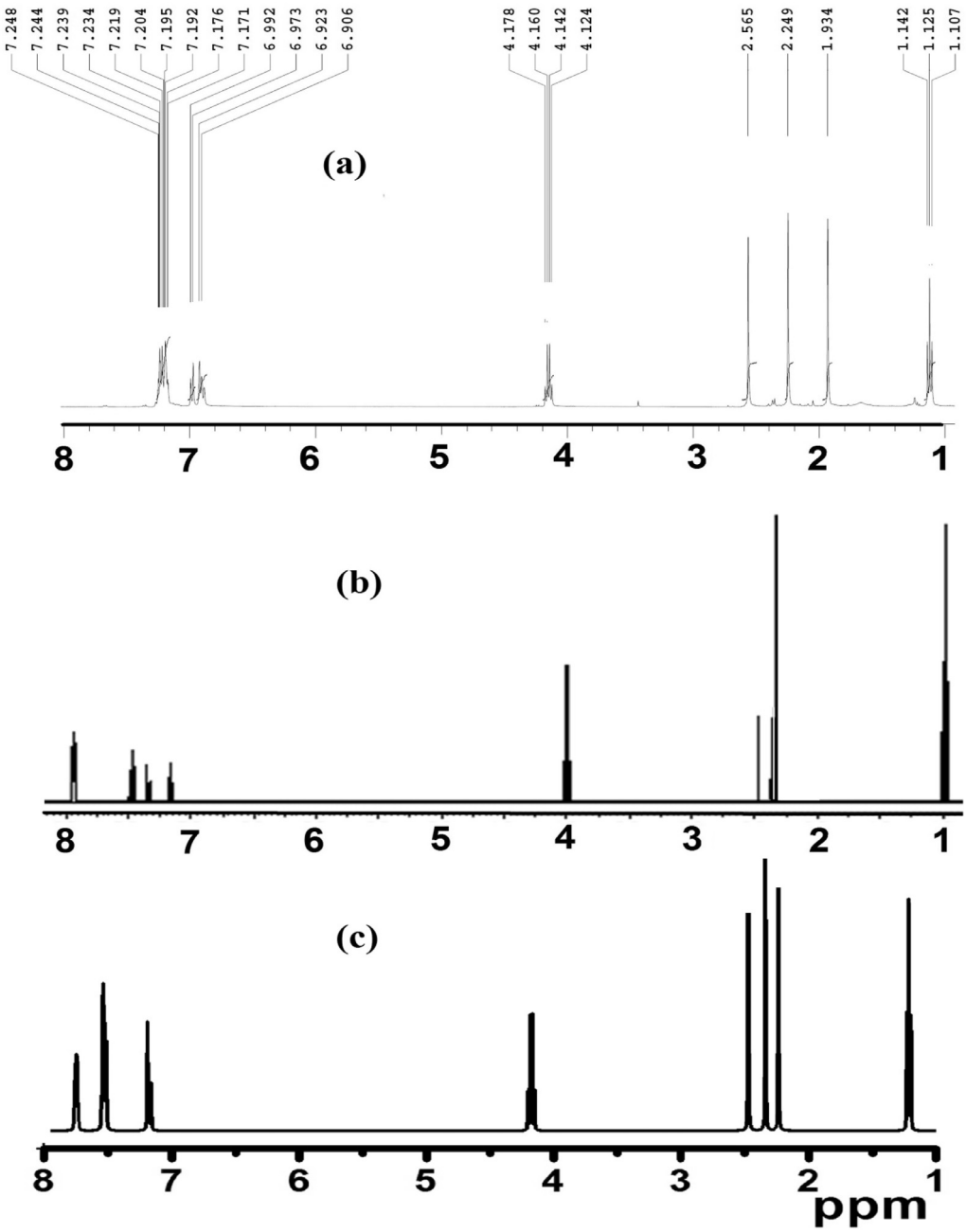

Fig. 8. ^{1}H NMR spectra of compound: (a) Experimental in $CDCl_3$, (b) Theoretical using ACD-lab and (c) Theoretical using NMR-DB compared with the experimental.

3.5. FT-IR spectral studies

The experimental IR spectrum illustrate the presence of several characteristic bands of stretching vibrations like aromatic C-H, aliphatic C-H (CH_3 and CH_2), C=O, C=N, C-N, C-O and N-N main functional groups (Fig. 10a). The theoretical DFT-IR spectrum showed slightly higher absorptions compared to the experimental stretching vibrations (Fig. 10b). For the title compound, C-H stretching vibrations of the phenyl rings are assigned in the range 3120–3035 cm^{-1} and 3200–3100 cm^{-1} theoretically. The stretching modes of the methylene CH_2 and methyl CH_3 groups are assigned at 3035-2980 cm^{-1} (theoretically) and at 2970-2875 cm^{-1}, 1100–1450 cm^{-1} (wagging, twisting and scissoring modes). The stretching mode of C=O assigned at 1780 cm^{-1} in the IR spectrum and at 1720 cm^{-1} theoretically. The IR spectral data of the compound is in good agreement with the reported structurally related molecule, ethyl 3-(4-methylbenzoyl)-4-phenyl-1*H*-pyrazole-5-carboxylate [38], which showed the absorption band at 1709 cm^{-1} for ester C=O stretching and at 1555 cm^{-1} for C=N stretching of pyrazole ring, the other absorption bands in the respective region.

The C=N stretching mode is assigned at 1550 cm^{-1} in the IR spectrum and at 1580 cm^{-1} theoretically. The C-N stretching vibrations are assigned in the region 1310 cm^{-1}, the band at 1360 cm^{-1} (DFT). The C-O stretching frequencies are observed at 1185 cm^{-1} in FT-IR spectrum and at 1210 cm^{-1} (DFT). The N-N stretching mode is assigned at 1090 cm^{-1} experimentally and at 1125 cm^{-1} theoretically. The other stretching and bending functional groups vibrations were cited to their expected positions. Graphical correlation between the experimental determined IR and DFT/B3LYP/6-311G(d)

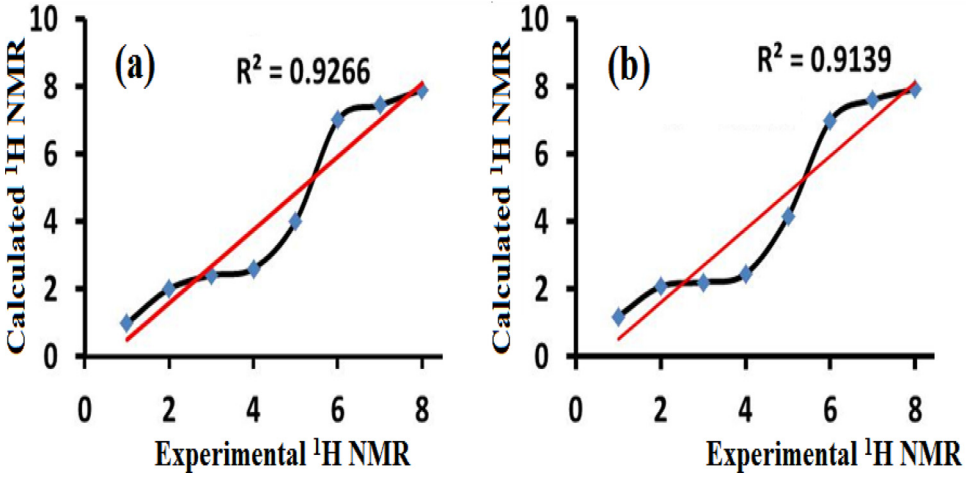

Fig. 9. (a) Experimental ^{1}H NMR *vs*. theoretical ACD-LAB and (b) Experimental ^{1}H NMR *vs*. theoretical NMR-DB.

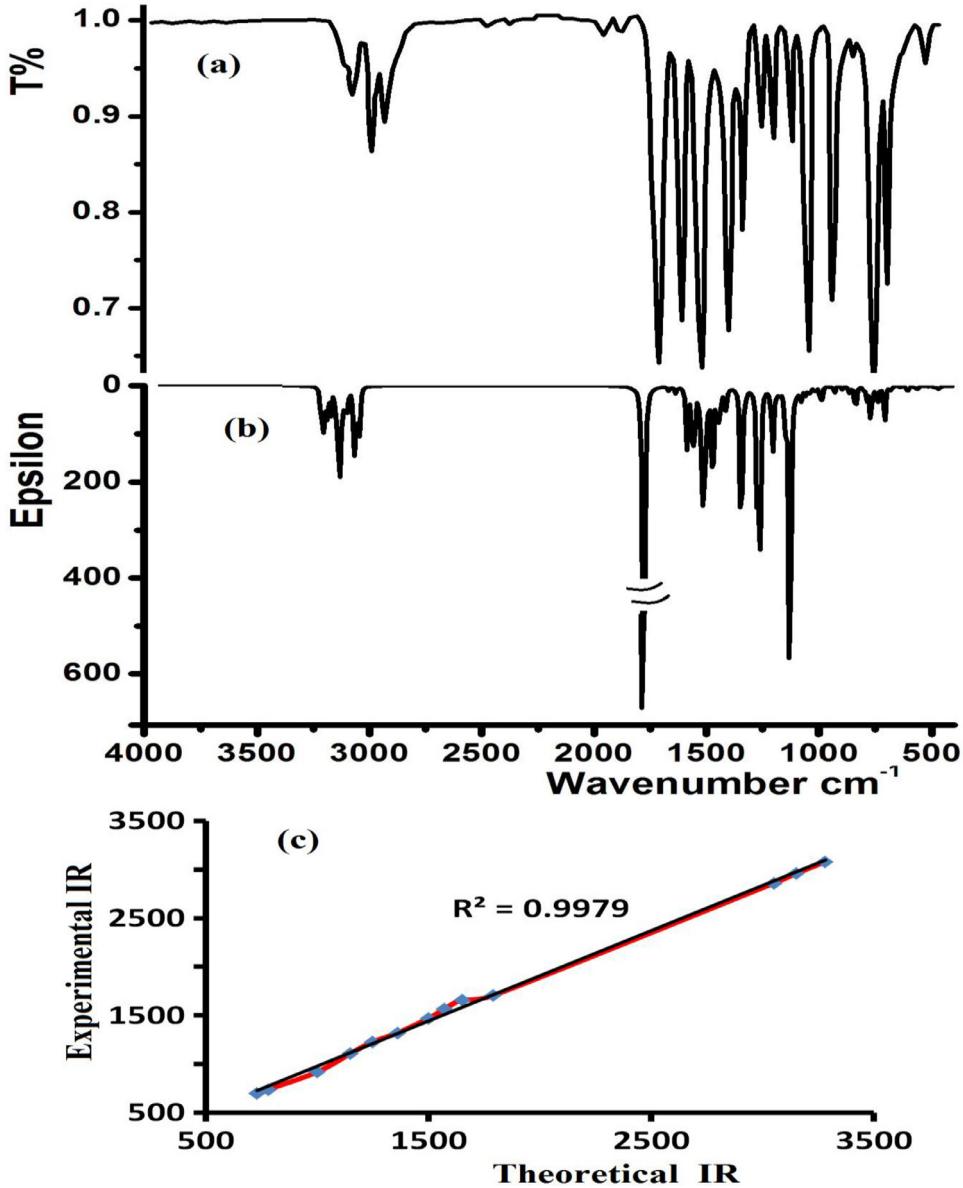

Fig. 10. FT-IR spectra of the compound, (a) experimental (b) DFT/B3LYP/6-31G(d) theoretical and (c) graphical correlation between experimental and theoretical IR data.

Table 3
All the experimental XRD torsion angles (°) with their DFT/B3LYP/6–311G(d) calculated values.

Torsion angles				Exp. XRD	B3LYP/6–31 G(d)
C3	N1	N2	C1	0.5	-0.25
C14	N1	N2	C1	176.5	178.12
N2	N1	C3	C2	-0.1	0.14
N2	N1	C3	C5	179.9	179.51
C14	N1	C3	C2	-175.6	-177.99
C14	N1	C3	C5	4.4	1.37
N2	N1	C14	C15	74.9	73.5
N2	N1	C14	C19	-101.6	-103.38
C3	N1	C14	C15	-109.8	-108.45
C3	N1	C14	C19	73.7	74.67
N1	N2	C1	C2	-0.6	0.25
N1	N2	C1	C4	178.2	179.64
C12	O2	C11	O1	-3.9	0.31
C12	O2	C11	C2	178.5	179.21
C11	O2	C12	C13	158.5	-176.29
N2	C1	C2	C3	0.6	-0.17
N2	C1	C2	C11	178.3	176.13
C4	C1	C2	C3	-178.2	-179.5
C4	C1	C2	C11	-0.4	-3.2
C1	C2	C3	N1	-0.2	0.01
C1	C2	C3	C5	179.8	-179.26
C11	C2	C3	N1	-177.8	-175.92
C11	C2	C3	C5	2.2	4.81
C1	C2	C11	O1	11.6	10.07
C1	C2	C11	O2	-170.9	-168.82
C3	C2	C11	O1	-171.3	-174.66
C3	C2	C11	O2	6.3	6.46
N1	C3	C5	C6	-129.8	-124.69
N1	C3	C5	C10	49.8	54.67
C2	C3	C5	C6	50.2	54.48
C2	C3	C5	C10	-130.2	-126.16
C3	C5	C6	C7	180	179.16
C10	C5	C6	C7	0.4	-0.22
C3	C5	C10	C9	-179.5	-179.36
C6	C5	C10	C9	0.2	0.01
C5	C6	C7	C8	-0.5	0.21
C6	C7	C8	C9	0.1	0
C7	C8	C9	C10	0.4	-0.2
C8	C9	C10	C5	-0.5	0.2
N1	C14	C15	C16	-177.4	-178.49
C19	C14	C15	C16	-1	-1.62
N1	C14	C19	C18	177.6	178.72
N1	C14	C19	C20	-0.2	-0.36
C15	C14	C19	C18	1.2	1.93
C15	C14	C19	C20	-176.5	-177.16
C14	C15	C16	C17	0.9	0.28
C15	C16	C17	C18	-1.2	0.66
C15	C16	C17	C21	178.4	179.61
C16	C17	C18	C19	1.5	-0.31
C21	C17	C18	C19	-178.1	-179.26
C17	C18	C19	C14	-1.5	-0.97
C17	C18	C19	C20	176.2	178.13

theoretical one is shown in Fig. 10c. Significant R^2 value 0.9979 was collected reflecting the excellent matching between theoretical and experimental IR analysis.

3.6. Exponential electronic and theoretical TD-SCF/DFT spectra

Electronic spectrum of the prepared compound was measured in CH_2Cl_2 and MeOH solvents (Fig. 10a). The λ_{max} = 250 nm as strong absorption band (π - π^* electron transition) appeared when both solvents was used, no other bands were detected elsewhere; moreover, no changes on the λ_{max} values recorded by changing the use of CH_2Cl_2 to MeOH which reflected the solvents affectlessness. The TD-SCF theoretical calculations in gaseous state, CH_2Cl_2 and MeOH solvents were performed to be compared with the exponential UV result, as shown in Fig. 11b. In gaseous state λ_{max} = 248 nm, in CH_2Cl_2 λ_{max} = 248 nm and in MeOH λ_{max} = 253 nm. No solvent effect on λ_{max} was detected in gaseous state nor in CH_2Cl_2 solvent (same values). In MeOH solvent, very small bathochromic shift (~ 5 nm) was detected theoretically compared to the gaseous state. In general, negligible solvent effect can be summarized by comparing experimental with theoretical analysis.

Table 4
Calculated frontier molecular orbital energies and electronic properties of the title compound.

Parameters	Value [B3LYP/6-311G(d,p)] (eV)
E_{HOMO}	- 6.26787
E_{LUMO}	- 0.89553
E_g	5.37235
Ionization potential (I)	6.26787
Electron affinity (A)	0.89553
Electronegativity (χ)	3.58170
Chemical hardness (η)	2.68617
Global softness (σ)	0.18614
Electrophilicity (ω)	2.38789
Chemical potential(μ)	- 3.58170
Dipole moment (Debye)	4.5806

where, χ = (I+A)/2, η = (I-A)/2, $\sigma = 1/\eta$ and $\omega = \mu^2/2\eta$, $E_g = E_{LUMO} - E_{HOMO}$.

3.7. Electronic properties and HOMO-LUMO

The electronic parameters were calculated and tabulated in Table 4. The electron affinity related to LUMO energy degree of electrons acceptation. Meanwhile, ionization potential of molecule concerning directly with HOMO energy reflects the electron donation capacity. The HOMO→LUMO orbital diagram is seen in Fig. 12. With the aid of DFT the electrophilicity (ω), electronegativity (χ), softness (σ) and hardness (η) of the molecule can be estimated [40,41]. The molecular orbital energy levels together with their energy gap (5.37235 eV) are in agreement with the experimental UV-result.

The value of chemical potential (-3.58170 eV) reflected the stability of the molecule. The hardness of the compound (2.68617 eV) made it a soft with faster electron transfer. Electronegativity and electrophilicity values revealed the compound with high electronic attraction power.

3.8. Analysis of molecular electrostatic potential surface

The MEP calculation of optimized structure of the compound was performed on DFT/B3LYP 6-311G (d), as seen in Fig. 13. The blue and red colours indicating the H-acceptor and H-donor sites respectively, construct the H-bonding interactions type and number. The electrons availability is decreased in the following order: red<orange<yellow<green<blue [42,43]. The MEP graph indicated carbonyl (O) and ester (O) with the red colour reveals the negative region and such atoms with their free lone pair of electrons as the best H-bond acceptor sites. This result is consistent with the HSA and X-ray packing data. It was very interesting to find the N atoms site with green and not red color on the MEP surface, which reflected the poorness degree in the free electrons of such atoms, this make the N atoms not suitable as H-bond acceptor sites. N=N….H hydrogen bonds were detected by X-ray and HSA data, this fact is in agreement with this data. The green colour of the CH hydrogen atoms reflected it as nucleophilic favored sites.

3.9. Mulliken atomic charge population analysis

The charge distribution of donor and acceptor atoms in molecules affects parameters like: dipole moment, polarizability,

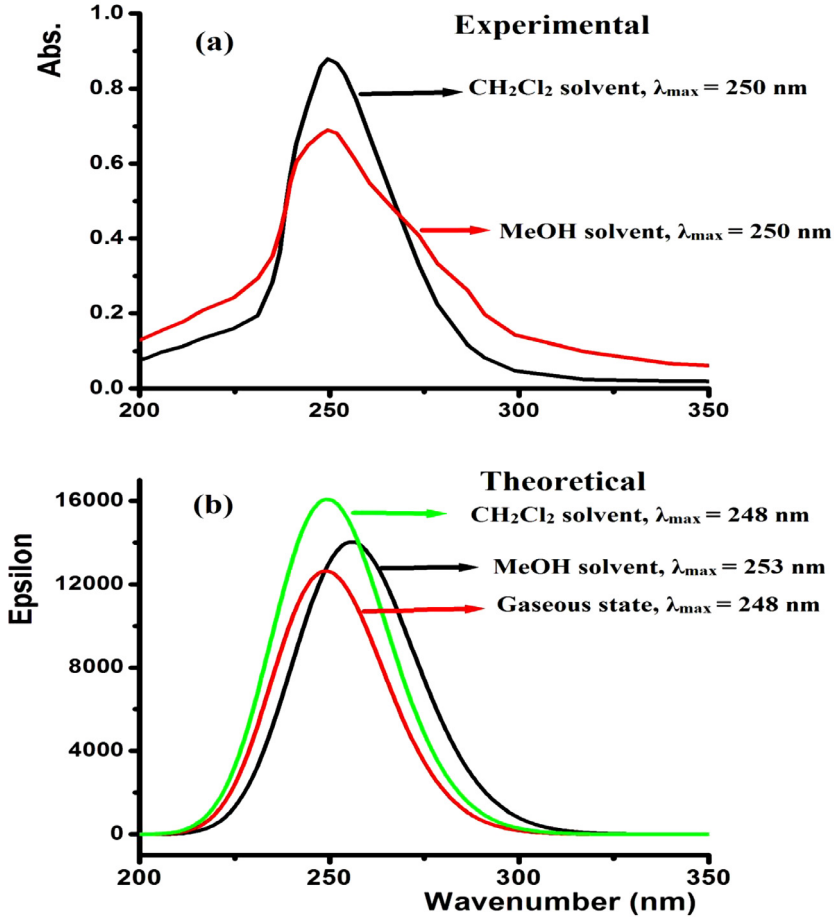

Fig. 11. The electronic spectra of the title compound (a) experimentally and (b) theoretical (TD-SCF/DFT).

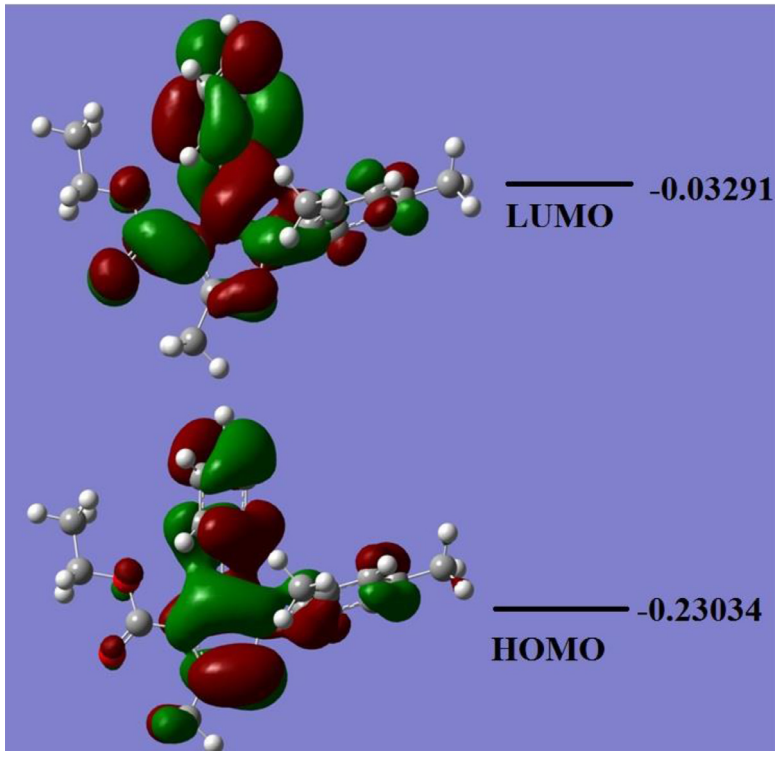

Fig. 12. Molecule HOMO-LUMO shape and energy diagram.

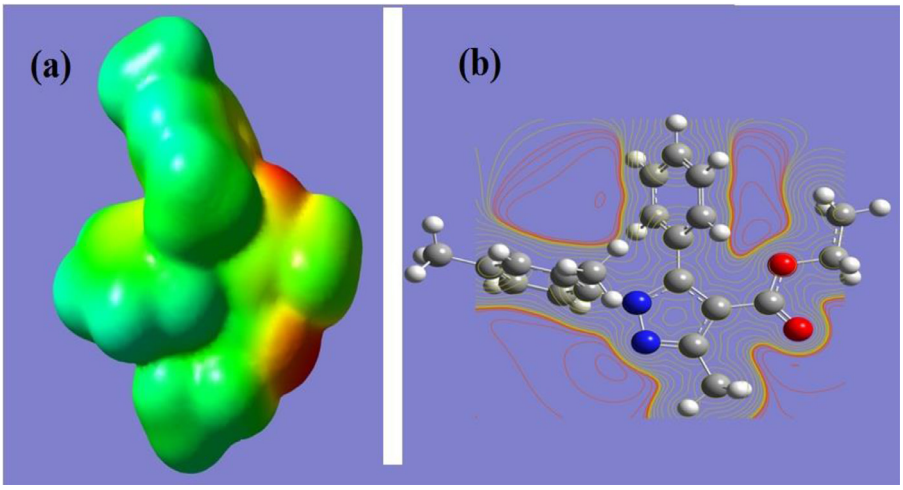

Fig. 13. (a) The MEP view and (b) the contour map of the desired compound.

refractivity and electronic structural. Mulliken population charge analysis was carried out through B3LYP/6-31G(d,p) level of theory, as seen in Table 5 and Fig. 14. The analysis was carried out into two ways: full charge calculation, all the atoms including the hydrogen atoms, as seen in Fig. 14**a,** on the other side hydrogen atoms were summed to the heavy atoms bind it, as seen in Fig. 14b. The calculation in general revealed the presence of several atoms with nucleophilic and electrophilic properties.

The analysis revealed the high electronegativity O and N atoms with their expected nucleophilicity amounts ~ -0.35e to -0.55e. The electrophilic mostly are localized at the hydrogen atoms ~ +0.05-0.18e values, the largest positive charge H atom was found on H46 with ~ 0.18e. The carbon atoms in the molecule have both positive and negative charges reflecting their poisons in the molecule, for example, C23 atom revealed the largest positive charge with ~ +0.55e, since it is ester carbon. Furthermore, all the four CH_3 carbon atoms showed the highest nucleophilicity with ~ 0.49e value, as seen in Fig. 14a.

3.10. Antioxidant screening: DPPH and Hydroxyl radical scavenging activity studies

In search of new potent antioxidant molecules, we successfully carried out cyclocondensation reaction of ethyl 1-(2,4-dimethylphenyl)-3-methyl-5-phenyl-1*H*-pyrazole-4-carboxylate. The prepared compound was evaluated for *in vitro* DPPH and Hydroxyl inhibitory activity method in triplicate. Both methods of antioxidant screening were performed in order to make sure the results converge and get a better method set up. Preliminary investigation of DPPH and hydroxyl scavenging activity in comparison with the ascorbic acid and butylated hydroxyanisole, respectively reference is illustrated in Fig. 15. The inhibition activity at the several concentrations 20 mM, 40 mM, 60 mM, 80 mM and 100 nM are listed in Table 6.

The antioxidant results of the title compound clearly showed that the freshly synthesized compound exhibited very good antioxidant activities especially at low concentrations. At concentrations of 20 mM and 40 mM, the desired compound behaved in its antioxidant activity mostly like the reference. This is good for application, since low dose of chemical can be introduced. As expected, by increasing the concentrations of the materials the antioxidant increased but not drastically. For example; in DPPH, moving from concentration 20 mM to 60 mM cased only 4% increase in the

Table 5
Mulliken charges of atoms in the title compound.

No.	Atom	Charge	No.	Atom	Charge
1	N	-0.4491	1	N	-0.4491
2	N	-0.3536	2	N	-0.3536
3	O	-0.5058	3	O	-0.5058
4	O	-0.4865	4	O	-0.4865
5	C	0.25775	5	C	0.25775
6	C	-0.141	6	C	-0.141
7	C	0.28551	7	C	0.28551
8	C	-0.4505	8	C	0.07109
9	H	0.16404	12	C	0.10463
10	H	0.17556	13	C	0.00036
11	H	0.182	15	C	-0.0095
12	C	0.10463	17	C	0.01565
13	C	-0.0973	19	C	-0.0031
14	H	0.09762	21	C	-0.0144
15	C	-0.1131	23	C	0.55905
16	H	0.10355	24	C	0.28776
17	C	-0.0871	27	C	0.03088
18	H	0.1027	31	C	0.17863
19	C	-0.1079	32	C	0.04046
20	H	0.1048	34	C	-0.0811
21	C	-0.1137	36	C	0.15272
22	H	0.09933	37	C	-0.1539
23	C	0.55905	39	C	0.14795
24	C	-0.0416	40	C	0.04251
25	H	0.17134	44	C	0.02306
26	H	0.15805			
27	C	-0.4661			
28	H	0.16465			
29	H	0.15852			
30	H	0.17382			
31	C	0.17863			
32	C	-0.062			
33	H	0.10242			
34	C	-0.1742			
35	H	0.09309			
36	C	0.15272			
37	C	-0.2349			
38	H	0.08101			
39	C	0.14795			
40	C	-0.4908			
41	H	0.16159			
42	H	0.18765			
43	H	0.18403			
44	C	-0.4923			
45	H	0.16225			
46	H	0.18013			
47	H	0.17292			

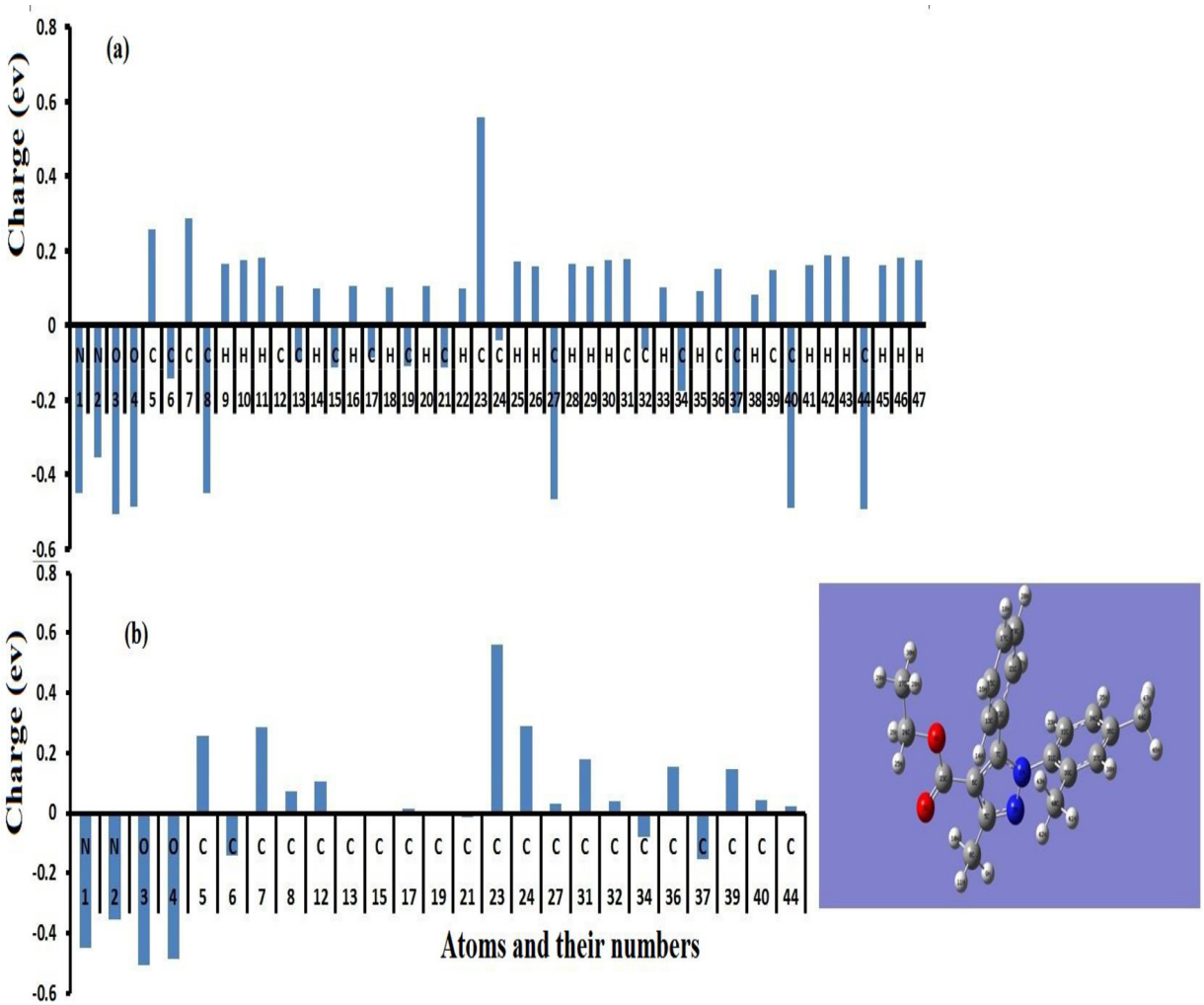

Fig. 14. Mulliken charges distribution (a) for all atoms including atoms and (b) the hydrogen atoms were summed to the heavy atoms.

Table 6
DPPH and hydroxyl radical scavenging activities of the designed compound

% DPPH radical scavenging					
	20 (μg/mL)	40 (μg/mL)	60 (μg/mL)	80 (μg/mL)	100 (μg/mL)
	13.20±0.54	14.87±0.21	17.65±0.12	20.40±0.87	23.21±0.65
Ascorbic acid	15.08±0.89	16.87±0.89	21.98±0.31	24.25±0.22	28.65±0.98
% Hydroxyl radical scavenging					
Compound	13.43±0.87	14.32±0.01	19.32±0.11	23.67±0.07	26.72±0.93
Butylated hydroxyanisole	13.87±0.10	17.95±0.12	25.58±0.20	32.03±0.32	36.87±0.76

activity. Interestingly, the synthesized compound shows better antioxidant properties in both the methods (Table 6) comparable with the similar structurally related pyrazole molecules at similar concentrations [44]. For instance, already reported compounds 1-(2,4-dimethoxy-phenyl)-3-(1-phenyl-3-p-tolyl-1*H*-pyrazol-4-yl)-propenone, and 3-[3-(2-chloro-phenyl)-1-phenyl-1*H*-pyrazol-4-yl]-1-(2,4-dimethoxy-phenyl)-propenone show the percentage inhibition of 13.5, and 13.8, respectively [45]; while the compounds 3-(4-bromophenyl)-1-(4-chlorophenyl)-4-(4,5diphenyl-1*H*-imidazol-2-yl)-1*H*-pyrazole, 1,3-bis(4-chlorophenyl)-4-(4,5-diphenyl-1*H*-imidazol-2-yl)-1*H*-pyrazole, and 3-(2-bromophenyl)-4-(4,5-diphenyl-1*H*-imidazol-2yl)-1-(p-tolyl)-1*H*-pyrazole, have the radical scavenging abilities of 2.0, 2.0, and 10.2%, respectively [46].

The two methods revealed a very close antioxidant result; the structure of the desired compound is stable enough to scavenge the free electron for both methods without side reactions cased structure decomposition. The radical-scavenging ability is commonly regarded as the basic property of an antioxidant and evaluated by trapping DPPH and Hydroxyl radical in this work. The absorbance of free radicals decreases in presence of the tested compound indicating their antioxidant potentials. The antioxidant activity of the compounds is related with their electron or hydrogen radical releasing ability to DPPH or Hydroxyl, so that they become stable diamagnetic molecules, which might be the reason for the higher antioxidant activity of the synthesized compound. Antioxidant activity of the compounds is also well explained by E_{HOMO}

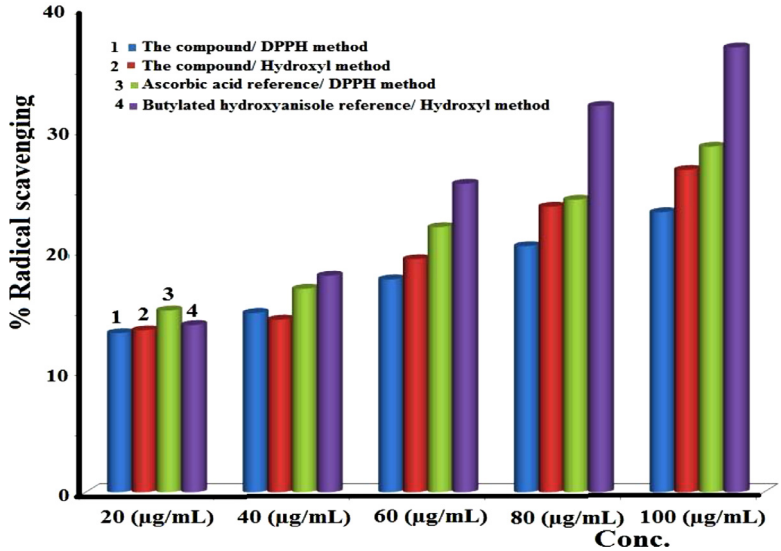

Fig. 15. DPPH and Hydroxyl radical scavenging activities.

and E_{LUMO}, as the electron donation property has been strongly attributed to E_{HOMO} (electron donation capability) and E_{LUMO} (electron accepting capability) [45]. The synthesized compound has higher E_{HOMO} and E_{LUMO} and therefore it is an effective agent for stabilizing the DPPH, and Hydroxyl radicals.

4. Conclusions

In the present work, ethyl 1-(2,4-dimethylphenyl)-3-methyl-5-phenyl-1*H*-pyrazole-4-carboxylate was prepared by Knoevenagel condensation reaction. The title compound was characterized spectroscopically and the structure was confirmed by single crystal X-ray diffraction studies. The crystal structure is stabilized by intermolecular hydrogen bond of the type C-H...O and $\pi \bullet\bullet\bullet \pi$ stacking interactions. Further, the optimized theoretical structure parameters were compared with the experimental X-ray structure. The calculated results of ^{1}H-NMR, TD-SCF, HOMO/LUMO, MEP, Hirshfeld surface and Mullikan population analysis are in good agreement with the experimental data. The MEP analysis revealed the high electronegativity of O and N atoms with their expected nucleophilicity amounts ~ -0.35e to -0.55e. The compound was evaluated *in vitro* for its antioxidant susceptibilities through DPPH and hydroxyl methods. *In vitro* DPPH and Hydroxyl radical scavenging assay results showed that the designed compound acts as a potential antioxidant.

5. Supplementary data

CCDC 2018644 contains the supplementary crystallographic data for the title compound. This data can be obtained free of charge via http://www.ccdc.cam.ac.uk/conts/retrieving.html, or from the Cambridge Crystallographic Data Centre, 12 Union Road, Cambridge CB2 1EZ, UK; fax: (+44) 1223-336-033; or e-mail: deposit@ccdc.cam.ac.uk.

Declaration of Competing Interest

All authors declare no conflict of interest including financial, personal or other relationships with other people or organizations for this article.

CRediT authorship contribution statement

S. Naveen: Conceptualization, Formal analysis, Software, Writing - original draft. **Karthik Kumara:** Formal analysis, Writing - original draft, Software, Validation. **A. Dileep Kumar:** Data curation, Formal analysis, Visualization. **K. Ajay Kumar:** Conceptualization, Methodology, Resources, Investigation. **Abdelkader Zarrouk:** Formal analysis, Data curation, Visualization. **Ismail Warad:** Conceptualization, Investigation, Software, Validation, Writing - original draft. **N.K. Lokanath:** Conceptualization, Supervision, Writing - review & editing.

Acknowledgments

The authors are grateful to the IOE Instrumentation Facility and National diffractometer facility, Department of Studies in Physics, University of Mysore, for providing the spectral and X-ray diffraction data.

References

[1] M.E. Buyukokuroglu, I. Gulcin, M. Oktay, O.I. Kufrevioglu, Pharmacol. Res. 44 (2001) 491–494.
[2] R. Nagamallu, B. Srinivasan, M.B. Ningappa, K. Ajay Kumar, Bioorg. Med. Chem. Lett. 26 (2016) 690–694.
[3] Y. Kaddouri, F. Abrigach, El.B. Yousfi, M. El Kodadi, R. Touzani, Heliyon 6 (2020) e03185.
[4] N. Renuka, H.K. Vivek, G. Pavithra, K. Ajay Kumar, Russ. J. Bioorg. Chem. 43 (2017) 197–210.
[5] J. Rangaswamy, H. Vijay Kumar, S.T. Harini, N. Naik, Bioorg. Med. Chem. Lett. 22 (2012) 4773–4777.
[6] E.A. Musad, R. Mohamed, B.A. Saeed, B.S. Vishwanath, K.M. Lokanatha Rai, Bioorg. Med. Chem. Lett. 21 (2011) 3536–3540.
[7] P.-Z. Li, Z.-Q. Liu, Tetrahedron 69 (2013) 9898–9905.
[8] A. Padmaja, C. Rajasekhar, A. Muralikrishna, V. Padmavathi, Eur. J. Med. Chem. 46 (2011) 5034–5038.
[9] A. Padmaja, T. Payani, G.D. Reddy, V. Padmavathi, Eur. J. Med. Chem. 44 (2009) 4557–4566.
[10] V. Sharath, H. Vijay Kumar, N. Naik, J. Pharm. Res. 6 (2013) 785–790.
[11] A. Burguete, E. Pontiki, D. Hadjipavlou-Litina, R. Villar, E. Vicente, B. Solano, S. Ancizu, S. Perez-Silanes, I. Aldana, A. Monge, Bioorg. Med. Chem. Lett. 17 (2007) 6439–6443.
[12] J. Prabhashankar, V.K. Govindappa, A.K. Kariyappa, Turk. J. Chem. 37 (2013) 853–857.
[13] F.S. Al-Saleh, I.K. Al Khawaja, J.A. Joule, J. Chem, Soc. Perkin Trans. 1 (1981) 642–645.
[14] A.A. EL-Sayed, M. Ohta, Bull. Chem. Soc. 46 (1973) 947–949.
[15] K. Mohanan, A.R. Martin, L. Toupet, M. Smietana, J.-J. Vasseur, Angew. Chem. Int. Ed. 49 (2010) 3196–3199.

[16] Z. Sui, J. Guan, M.P. Ferro, K. McCoy, M.P. Wachter, W.V. Murray, M. Singer, M. Steber, D.M. Ritchie, D.C. Argentieri, Bioorg. Med. Chem. Lett. 10 (2000) 601–604.
[17] S.R. Stauffer, C.J. Coletta, R. Tedesco, G. Nishiguchi, K. Carlson, J. Sun, B.S. Katzenellenbogen, J.A. Katzenellenbogen, J. Med. Chem. 43 (2000) 4934–4947.
[18] G. Vasanth Kumar, M. Govindaraju, N. Renuka, G. Pavithra, B.N. Mylarappa, K. Ajay Kumar, Int. J. Pharm. Sci. Res. 3 (12) (2012) 4801–4806.
[19] Z. Christina, D. Florea, D. Constantin, I. Mircea, M. Maria, T. Isabela, M.N. George, Ind. J. Chem. 53B (2014) 733–739.
[20] R. Katoch-Rouse, O.A. Pavlova, T. Caulder, A.F. Hoffmann, A.G. Mukhin, A.G. Horti, J. Med. Chem. 46 (2003) 642–645.
[21] V. Kumar, K. Kaur, G.K. Gupta, A.K. Sharma, Eur. J. Med. Chem. 69 (2013) 735–753.
[22] C. Lamberth, Heterocycles 71 (2007) 1467–1502.
[23] M.J. Frisch, G.W. Trucks, H.B. Schlegel, G.E. Scuseria, M.A. Robb, J.R. Cheeseman, G. Scalmani, V. Barone, B. Mennucci, G.A. Petersson, H. Nakatsuji, M. Caricato, X. Li, H.P. Hratchian, A.F. Izmaylov, J. Bloino, G. Zheng, J.L. Sonnenberg, M. Hada, M. Ehara, K. Toyota, R. Fukuda, J. Hasegawa, M. Ishida, T. Nakajima, Y. Honda, O. Kitao, H. Nakai, T. Vreven, J.A. Montgomery Jr., J.E. Peralta, F. Ogliaro, M. Bearpark, J.J. Heyd, E. Brothers, K.N. Kudin, V.N. Staroverov, T. Keith, R. Kobayashi, J. Normand, K. Raghavachari, A. Rendell, J.C. Burant, S.S. Iyengar, J. Tomasi, M. Cossi, N. Rega, J.M. Millam, M. Klene, J.E. Knox, J.B. Cross, V. Bakken, C. Adamo, J. Jaramillo, R. Gomperts, R.E. Stratmann, O. Yazyev, A.J. Austin, R. Cammi, C. Pomelli, J.W. Ochterski, R.L. Martin, K. Morokuma, V.G. Zakrzewski, G.A. Voth, P. Salvador, J.J. Dannenberg, S. Dapprich, A.D. Daniels, O. Farkas, J.B. Foresman, J.V. Ortiz, J. Cioslowski, D.J. Fox, Gaussian 09, Revision B.01, Gaussian, Inc., Wallingford, CT, 2010.
[24] A. Frisch, R. Dennington, T. Keith, J. Millam, A. Nielsen, A. Holder, J. Hiscocks, GaussView Version 5 User Manual, Gaussian Inc., Wallingford, CT, USA, 2009.
[25] M.J. Turner, J.J. McKinnon, S.K. Wolff, D.J. Grimwood, P.R. Spackman, D. Jayatilaka, M.A. Spackman, CrystalExplorer (Version 17.5), University of Western Australia, 2018.
[26] (a) G.M. Sheldrick, Acta Cryst. C71 (2015) 3–8; (b) G.M. Sheldrick, Acta Cryst. A46 (6) (1990) 467–473.
[27] A.L. Spek, Acta. Cryst. A. 46 (1990) C34.
[28] C.F. Macrae, I.J. Bruno, J.A. Chisholm, P.R. Edgington, P. McCabe, E. Pidcock, L.M. Rodriguez, R. Taylor, J. van de Streek, P.A. Wood, J. Appl. Cryst. 41 (2008) 466–470.
[29] K.R. Raghavendra, N. Renuka, V.H. Kameshwar, B. Srinivasan, K.A. Kumar, S. Shashikanth, Bioorg. Med. Chem. Lett 26 (2016) 3621–3625.
[30] S. Naveen, K. Kumara, H.M. Al-Maqtari, M.V. Deepa Urs, J. Jamalis, K.R. Reddy, N.K. Lokanath, Chem. Data Coll. 24 (2019) 100292.
[31] D.M. Lokeshwari, A. Dileep Kumar, S. Bharath, S. Naveen, N.K. Lokanath, K. Ajay Kumar, Bioorg. Med. Chem. Lett. 27 (2017) 3806–3811.
[32] M.G. Prabhudeva, S. Bharath, A. Dileep Kumar, S. Naveen, N.K. Lokanath, B.N. Mylarappa, K. Ajay Kumar, Bioorg. Chem. 73 (2017) 109–120.
[33] K. Kumara, S. Naveen, L.D. Mahadevaswamy, K. Ajay Kumar, N.K. Lokanath, Chem. Data Coll. 9 (2017) 251–262.
[34] K. Kumara, A. Dileep Kumar, K. Ajay Kumar, N.K. Lokanath, Chem. Data Coll. 13-14 (2018) 40–59.
[35] V. Channabasappa, K. Kumara, N.K. Lokanath, A.K. Kariyappa, Chem. Data Coll. 15 (2018) 134–142.
[36] S.B. Benaka Prasad, S. Naveen, C.S. Ananda Kumar, N.K. Lokanath, A.V. Raghu, I. Dargameh, K.R. Reddy, I. Warad, J. Mol. Struct. 1167 (2018) 215–226.
[37] I. Warad, M.M. Abdoh, A.A. Ali, S. Naveen, Karthik Kumara, A. Zarrouk, N.K. Lokanath, J. Mol. Struct. 1154 (2018) 619–625.
[38] D. Nair, P. Pavashe, S. Katiyar, I.N.N. Namboothiri, Tet. Lett. 57 (2016) 3146–3149.
[39] A. Dileep Kumar, S. Bharath, R.N. Dharmappa, S. Naveen, N.K. Lokanath, K. Ajay Kumar, Res. Chem. Intermed. 44 (2018) 5635–5652.
[40] S. Xavier, S. Periandy, S. Ramalingam, Spectrochim. Acta A 137 (2015) 306–320.
[41] Karthik Kumara, A. Dileep Kumar, S. Naveen, K. Ajay Kumar, N.K. Lokanath, J. Mol. Struct. 1161 (2018) 285–298.
[42] C.S. Karthik, K. Kumara, S. Naveen, L. Mallesha, P. Mallu, M.V. Deepa Urs, N.K. Lokanath, J. Mol. Struct., 1224, 2021, 129077.
[43] J.-H. Zhou, L.-W. Zheng, M.-C. Yan, M.-J. Shi, J. Liu, G.-Q. Shangguan, J. Chem., 2017, Article ID 6537402. https://doi.org/10.1155/2017/6537402.
[44] E.M. Flefel, W.I. El-Sofany, M. El-Shahat, A. Naqvi, E. Assirey, Molecules 23 (2018) 2548.
[45] B.P. Bandgar, S.S. Gawande, R.G. Bodade, N.M. Gawande, C.N. Khobragade, Bioorg. Med. Chem. 17 (2009) 8168–8173.
[46] H. Brahmbhatt, M. Molnar, V. Pavic Karbala, Int. J. Mod. Sci. 4 (2018) 200–206.